NJC

Accepted Manuscript

This is an *Accepted Manuscript*, which has been through the Royal Society of Chemistry peer review process and has been accepted for publication.

Accepted Manuscripts are published online shortly after acceptance, before technical editing, formatting and proof reading. Using this free service, authors can make their results available to the community, in citable form, before we publish the edited article. We will replace this *Accepted Manuscript* with the edited and formatted *Advance Article* as soon as it is available.

You can find more information about *Accepted Manuscripts* in the Information for Authors.

Please note that technical editing may introduce minor changes to the text and/or graphics, which may alter content. The journal's standard Terms & Conditions and the Ethical guidelines still apply. In no event shall the Royal Society of Chemistry be held responsible for any errors or omissions in this *Accepted Manuscript* or any consequences arising from the use of any information it contains.

ROYAL SOCIETY OF CHEMISTRY

www.rsc.org/njc

NJC

PAPER

PTFE supported gold nanoparticles as photocatalyst for oxidative esterification of aldehydes.

Received 00th January 20xx,
Accepted 00th January 20xx

DOI: 10.1039/x0xx00000x

www.rsc.org/

Maël Penhoat,*[a,d] Théodore Vanbesien,[a,d] Adrien Cocud,[a,d] Ahmed Addad,[b,d] Hervé Vezin,[c,d] and Christian Rolando[a,d]

Homogeneous, small gold nanoparticles (d = 1.87 nm) have been prepared by photochemical reduction of $HAuCl_4$ in the presence of Irgacure® 2959 under high power UV irradiation at 365 nm produced by a LED source. These particles have been deposited on PTFE microbeads (d = 200 µm) and evaluated for the catalysis of the oxidative esterification of aldehydes in the presence of H_2O_2. Under green light (λ ≈ 530 nm) and repeated addition of H_2O_2, the catalytic system is accelerated and achieves complete conversions in minutes. Furthermore the catalyst can be recycled ten times consecutively without any activity lost by adding a step for AuNPs recycling. The mechanism of the reaction follows a zero rate order, Hammett free energy relationships for substituted benzaldehydes afforded a positive ρ value (ρ = 2.35) demonstrating that the initial hemiacetalisation equilibrium (ρ = 2.31) is the rate determining step. Kinetics data are in agreement with an Eley-Rideal type mechanism and permits to propose a reaction mechanism.

Introduction

Esterification reaction is traditionally a two-step procedure including, first, the preparation of an activated carboxylic acid derivative such as acid anhydride, acid chloride or *N*-hydroxyester under stoichiometric conditions, then their reaction with an alcohol to produce the corresponding ester.[1, 2] These protocols usually generate a large amount of waste. Recently, direct oxidative esterification reactions from alcohols or aldehydes catalyzed by reusable heterogeneous catalysts under mild conditions, appeared as attractive alternatives for both organic synthesis and green chemistry.[3]

Since the pioneering discovery by Haruta and coworkers who demonstrated that gold nanoparticles (AuNPs) catalyzes the oxidation of CO effectively at low temperatures,[4] the scope of gold catalyzed oxidation reactions has expanded tremendously.[5-7] In particular, the oxidation of alcohols into the corresponding acids has received significant attention.[8] Under similar conditions, oxidation of aldehydes to esters proceeds under mild conditions.[9-13] For this purpose, the use of molecular oxygen or hydrogen peroxide[14] in catalyzed oxidation reactions proved to be particularly effective as co-oxidant for AuNPs catalytic systems. These new catalytic systems satisfy most of the demands for a modern, sustainable and ‘‘green’’ oxidation reaction.

AuNPs exhibit a surface plasmon resonance (SPR) absorption band around 520 nm.[15] Excitation of the surface plasmon band was described recently as a strategy of choice in order to facilitate electronic transfers that occur along redox reactions.[16, 17] This photocatalytic activity of AuNPs has attracted increasing attention in recent years because it can be driven with sunlight at ambient temperatures.[18] The mechanism of AuNPs photocatalytic activity has been examined by Zhu *et al.* who gave a mechanism different from that for conventional semiconductor photocatalysts.[19]

In the continuity of our research program concerning the synthesis of gold nanoparticles within microreactors[20] and their immobilization into fused silica capillary tubings for the development of catalytic microreactors,[21] we recently observed that, submitted to colloidal AuNPs solution, Teflon® coated magnetic stirrer bars developed a purple–brown color on surface characteristic of gold nanoparticles deposition. We turned this observation in a reproducible protocol and we describe here the preparation and characterization of PTFE supported gold catalyst. In order to evaluate its catalytic efficiency, the photocatalyzed oxidative esterification of various substituted benzaldehydes in the presence of methanol under mild conditions has been evaluated. Traditional methods for the preparation of supported catalysts include co-precipitation, deposition-precipitation, ion-exchange, impregnation, and successive reduction and calcinations.[22] However, these methodologies have some disadvantages, such as lack of control

[a] Université de Lille, CNRS, USR 3290, MSAP, Miniaturisation pour la Synthèse l'Analyse et la Protéomique, F-59000 Lille, France - Email : mael.penhoat@univ-lille1.fr
[b] Université de Lille, CNRS, UMR 8207, UMET, Unité Matériaux et Transformations, F-59000 Lille, France
[c] Université de Lille, CNRS, UMR 8516, LASIR Laboratoire de Spectrochimie Infrarouge et Raman, F-59000 Lille, France
[d] Université de Lille, CNRS, FR 2638, Institut Eugène-Michel Chevreul, FR CNRS, F-59000 Lille, France

Electronic Supplementary Information (ESI) available: Additional data including characterization of colloidal AuNPs (DLS, UV-Vis), AuNPs/PTFE catalyst (XPS), catalytic experiments (GC-MS kinetic studies, Eley-Rideal fitting model, ^{1}H NMR hemiacetal equilibrium constant measurements, Hammett study). Binocular loop study concerning the evolution of AuNPs/PTFE morphology along catalytic experiments (with or without recycling procedure) is also included. See DOI: 10.1039/x0xx00000x

over size, morphology, especially for catalyst as AuNPs, with limited stability. Therefore, the immobilization of pre-synthesized AuNPs has gained attention; since it can lead to controllable size, shape and surface properties of nanoparticles.[23] By choosing the preparation method of the nanoparticles, such properties can be tuned as well as their catalytic activities. In the present study, pre-synthesized uncoordinated, small and homogeneous AuNPs (average diameter 1.87 nm), obtained by photochemical reduction of $HAuCl_4$ in presence of Irgacure® 2959, were used as precursors for the preparation of PTFE supported gold catalyst. These Teflon® supported particles were found to be excellent recyclable photocatalyst for the oxidation of substituted benzaldehydes to their corresponding methyl esters.

Experimental

Materials

All chemicals were used as received without any purification. Hydrogen tetrachloroaurate (III) hydrate 99.9%, Au 49% ($HAuCl_4$) was purchased from Strem Chemicals (Bischheim, France). All other chemical compounds were purchased from Sigma-Aldrich (Lyon, France). All solutions were prepared from deionized water produced by a Milli-Q® system from Millipore (Molsheim, France).

AuNPs photochemical synthesis

The preparation of gold nanoparticles was performed according to the original procedure reported by Scaiano *et al.*[24-26] Every reactions have been performed in an optical transparent plastic or quartz cuvette (12.5 × 12.5 × 45 mm). The irradiation source Lightning Cure LC-L1 equipped with L9613-200 lens (illumination diameter = 10 mm) from Hamamatsu (Massy, France) was placed on the top of the cuvette and used at a specified intensity (λ = 365 nm). Irradiance was measured in $mW.cm^{-1}$ with a Hamamatsu UV power meter (C6080) positioned at 1 cm from the source and was in accord with the power indicated by the source.

Typical procedure. All the experiments were performed at atmospheric pressure without exclusion of air by an inert gas. In a typical preparation, 2 mL of $HAuCl_4$ solution (6.6×10^{-4} M) are poured in a cuvette. Then, 2 mL of 4 - (2 - hydroxyethoxy)phenyl - (2 – hydroxyl – 2 - propyl)ketone (*Irgacure® 2959*) solution (2×10^{-3} M) were added to the cuvette. The obtained pale yellow solution was left under slow mechanical stirring for 2 minutes. When the solution is irradiated a red-ruby colloid solution developed with time. After complete reaction (15 minutes) the gold colloid solution is collected in an Erlenmeyer flask surrounded with aluminum foil and conserved at cold temperature (4 °C). The experiment is repeated 10 times to obtain a volume of about 40 mL for later immobilization on PTFE microbeads. The study of AuNPs average diameter *vs* irradiance of the UV light source has been performed for every samples according to this procedure by varying the light power in %.

AuNPs colloid solution Characterization. The UV-vis spectra of the AuNPs colloids were measured using a Cary UV 100 spectrophotometer from Varian (Massy, France). Dynamic Light Scattering (DLS) analysis was performed on a DynaPro NanoStar instrument Wyatt (Toulouse, France) at a thermostated temperature of 25 °C using a fixed scattering angle of 173 °.

TEM analysis has been performed on these samples using a FEI Tecnai G2 20 (Hillsboro, OR, USA) equipped with a LaB6 filament at 200 kV. The specimens for examination by electron microscopy were prepared by adding one or two drops of a colloïd solution of the nanoparticles onto holey carbon films supported on standard copper grids. In order to avoid any agglomeration process along deposition, a silicon dioxide grid (20 nm film, from SIMpore Inc., West Henrietta, NY, USA) functionalized in surface with 25 µL of mercaptopropyltriethoxysilane (Sigma, Saint Quantin-Fallavier, France) for 2 hours has been evaluated in place of standard copper grids.

AuNPs immobilization on PTFE microbeads

Typical procedure. Fifty mg of PTFE powder (particle diameter: 200 µm) was placed in a 50 mL glass Erlenmeyer. Then, 5 mL of acetone were poured into the Erlenmeyer. The Erlenmeyer was closed and mechanically shaken with a CAT S50 (Staufen, Germany) wrist arm shaker until no PTFE agglomerates remained. Then 5 mL of AuNPs colloids were added to the PTFE suspension. The suspension was shaken overnight. The purple-grey PTFE powder was then filtered under vacuum on a frit, washed 5 times with 5 mL of dry acetone and let dried over 15 minutes. This experiment has also been performed on larger quantities (50 mL) using similar ratios.

AuNPs/PTFE characterization. The AuNPs/PTFE has been characterized by MEB, XPS and EPR. XPS analyses were obtained on a VG ESCALAB 220XL instrument (Villebon-sur-Yvette, France). SEM images were obtained with a JEOL JSM-7800F LV (FEG, low vacuum) instrument (Tokyo, Japan). TEM images were recorded with a FEI Tecnai G2 20 instrument (Hillsboro, OR, USA) operating at 200 keV. EPR spectra were recorded using a Bruker (Wissembourg, France) Elexys E580 spectrometer operating at X-band modulation amplitude and microwave power were set respectively at 5 Gauss and 1 mW. Spectra were recorded at 5 K using a Bruker Cryofree system.

Oxidative esterification of benzaldehydes

Typical procedure under room light illumination conditions. In a typical procedure, 1.3 mmol of base (2 eq.) were dissolved in 10 ml of dry methanol and poured into a 20 ml flask. The mixture is stirred until complete dissolution of the base. Then, 0.64 mmol of benzaldehyde are added (1 eq. 65 µL) and the reaction mixture is let stirred for additional 30 minutes. Finally, 1 mmol (1.5 eq., 50 µL) of hydrogen peroxide ($50\%_{w/w}$ in water) and AuNPs/PTFE catalyst (200 mg, $1\%_{mol}$) are added to the mixture which define the starting time of the reaction. The reaction medium is strongly stirred during the reaction to disperse the solid catalyst into the solution. Every 20 minutes, 1 mmol (1.5 eq., 50 µL) of hydrogen peroxide ($50\%_{w/w}$ in water) are added. At the end of the reaction, the catalyst is filtered off on a frit, the solvent is evaporated under reduced pressure and the crude mixture is analyzed by ^1H NMR.

Kinetic monitoring. For kinetic monitoring 50 µL of the reaction medium are sampled at different times and introduced into a vial containing 2 µL of formic acid and 1 mL of CH_2Cl_2 to quench the reaction. The sample is then injected without further treatment into a GC-MS apparatus: PolarisQ Thermo Electron (electron ionization, EI 70 eV, column: Rxi®-5ms, length: 60 m; internal diameter: 0.25 mm; film thickness 0.5 µm). The GC method was the following: split 1/50, temperature gradient from 50 °C to 275 °C at 5 °C.min-1. Every kinetic measurements have been repeated 2 or 3 times and given values are averaged.

Photocatalytic procedures. For photocatalytic reactions with *t*-BuOK as the base, a green fluorescent tube lamp (LEXMAN, EQSS-3, 15W, 120 mA, E27) is placed in close contact with the Pyrex® flask before introducing the catalyst. The irradiation is maintained during all the reaction time and 1 mmol (1.5 eq., 50 µL) of hydrogen peroxide (50%$_{w/w}$ in water) are added every 8 minutes. For Hammett relationship experiments, the same procedure has been used with various *p*-substituted benzaldehydes (0.64 mmol). The same previous work-up and kinetic monitoring procedure have been used. Every kinetic measurements have been repeated 2 or 3 times and given values are averaged. For reaction under solar illumination conditions, the same procedure has been applied by placing the flask under magnetic stirring outside of the building (outside temperature: 31°C). The same previous work-up and kinetic monitoring procedure have been used.

Hemiacetalisation equilibrium constants measurements

Typical procedure. In a 15 mL flask, 0.1 mmol of *t*-BuOK (2 eq., 11 mg) and 0.05 mmol (1 eq.) of the para-substituted benzaldehyde are dissolved in CD_3OD (0.75 mL) and the mixture is stirred for 2 hours at room temperature. The mixture is transferred to a NMR tube and analyzed by ^1H NMR with a Bruker (Wissembourg, France) Advance 300 Ultrashield spectrometer at room temperature with calibration on the solvent peak. The equilibrium constant is determined by comparison of aromatic peaks, hemiacetalic and aldehydic peaks (averaged integration).

Catalyst recycling procedure

Typical procedure. In a 25 mL flask, previously used AuNPs/PTFE catalyst (250 mg) is introduced and consequently 5 mL of acetone and 5 mL of deionized water are added. Then 300 µL of H_2O_2 (50%$_{w/w}$ in water) are added and the mixture is stirred for two hours at room temperature. The catalyst is filtered on a frit, washed with methanol and dried before to be reused in the following catalytic run. Recycled AuNPs/PTFE catalyst has then been analysed by XPS and the evolution of morphology is followed step by step under a stereomicroscope (Nikon, SMZ 1000).

Results and discussion

Gold nanoparticles photochemical synthesis

The $HAuCl_4$/I-2959® samples were typically irradiated in a UV-Vis cuvette without air exclusion using a new generation of high power UV LED system (Hamamatsu LC-L1, Fig. 1) delivering a focalized irradiation of 350 mW.cm^{-2}, at 365 nm. The reaction was monitored by UV-Vis spectroscopy and dynamic light scattering (DLS) to determine the AuNPs size. The UV-Vis kinetic monitoring of the surface plasmon band (530 nm) showed that absorbance starts to increase after 3 minutes. The reaction arrived to completion after 13 minutes and followed a first order rate law, with a kinetic constant of 4.3×10^{-3} s^{-1} (Fig. 2). This result was confirmed by following the disappearance of the $HAuCl_4$ absorption band at 217 nm. The DLS monitoring confirmed the UV-Vis observation that the first measurable AuNPs appeared after 3 minutes. The AuNPs hydrodynamic diameter steadily increased from 1.10 nm at the beginning to 1.87 nm at the end of the reaction (Fig. 3b). This results confirms that a higher UV intensity led to AuNPs with a smaller diameter. DLS analysis showed two distinct populations (Fig. 3a); one major centered around 1.87 nm (99.8% weight) and a second minor centered around 31 nm (0.2% weight) confirming that AuNPs are nearly monodispersed. A particularly interesting advantage of this high power UV LED irradiation system concerns the possibility to adjust the illumination power at the desired value (0-100%). When varying the UV light intensity from 350 mW.cm^{-2} (100%) to 91 mW.cm^{-2} (25%), we observed a linear correlation between the measured average hydrodynamic diameter by DLS and the light intensity. Using this property, it is then possible to directly select the AuNPs diameter by applying the proper irradiation power according to the following equation:

$$d_{AuNPs} = -0.0384 \times I_{irr} + 14.64 \qquad R^2 = 0.97$$

where d is the AuNPs average hydrodynamic diameter in nanometers and I_{irr} corresponds to the light source irradiance in mW.cm^{-2} measured with an UV power meter (Hamamatsu – C6080) at 1 cm from the source.

Despite many efforts, TEM analysis of AuNPs colloid solution didn't furnish acceptable results. Indeed along deposition on TEM grids an agglomeration process is observed with the formation, on the border of the grid, of black vesicles corresponding to agglomerated 1-2 nm nanoparticles. In every cases only the second minor population (average diameter = 30 +/- 10 nm) presenting various shapes can be easily observed.

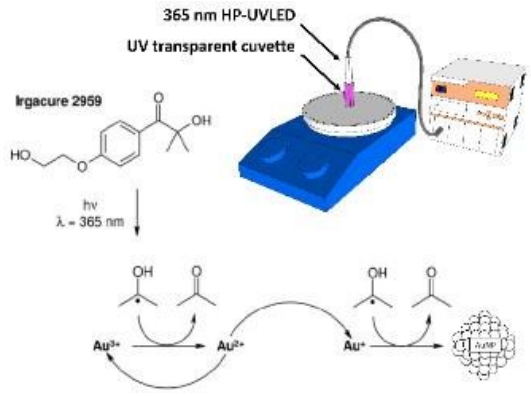

Fig. 1 AuNPs photochemical synthesis in the presence of Irgacure® 2959 using UV LED irradiation system (365 nm, 350 mW.cm^{-2}).

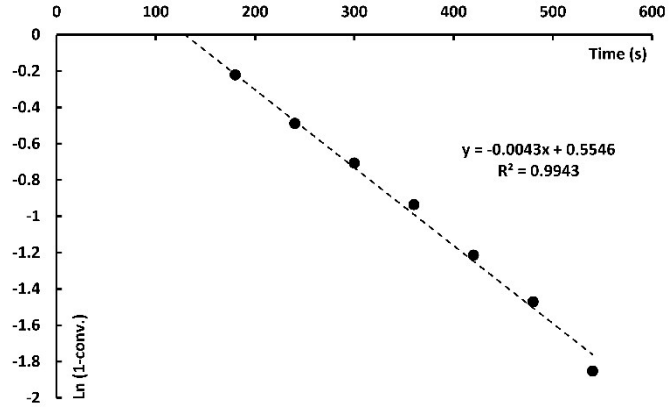

Fig. 2 UV-Vis kinetic measurement at 534 (± 2) nm for AuNPs photochemical synthesis.

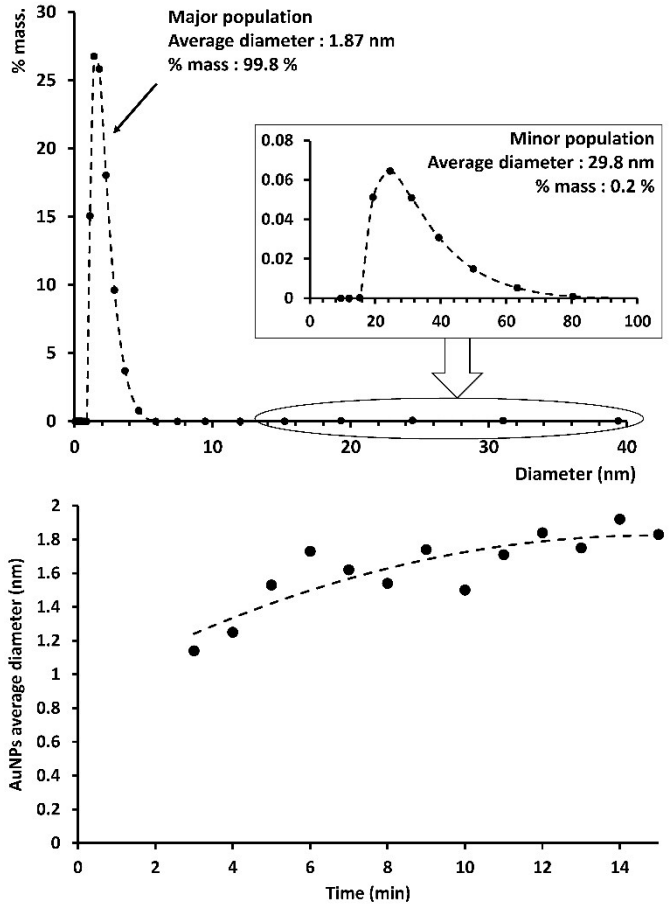

Fig. 3 (a) Upper panel. DLS measurement after 15 min. (b) Bottom panel. DLS monitoring of the major population.

It must be pointed out that most of the TEM analysis of AuNPs in the nanometer range are AuNPs stabilized by strong ligands (thiols,[27] phosphines,[28] amino terminated ionic liquid[29]) whereas our AuNPs are only weakly stabilized.

Gold nanoparticles immobilization on PTFE

Preliminary experiments showed that the Teflon coated magnetic bar used for mixing AuNPs during their photochemical synthesis becomes purple–brown on surface characteristic of AuNPs deposition, suggesting that Teflon® could be a new support for AuNPs catalysts. If the deposit of gold on PTFE surface is well-known either by ion beam assisted deposition on surface[30] or targeted electrochemical reduction of Au^{3+} solution[31] they are very few reports concerning the chemical anchoring of AuNPs on PTFE. Recently Redel *et al.* described the deposition of AuNPs on Teflon® surface by the UV irradiation of AuNPs/$BMIM^+BF_4^-$ solution in the presence of PTFE.[32] The authors detect an ESR signal in these AuNPs supported on PTFE particles. They assign this signal to a charge transfer between the AuNPs and the PTFE surface and the formation of (F···Au) interactions that explain the stability of the AuNPs on PTFE particles. These PTFE immobilized AuNPs have never been investigated as catalyst. Interestingly, PTFE is a support of choice for mild catalytic conditions. Indeed, its hydrophobic and inert character differs from the traditional AuNPs catalyst supports (TiO_2, SiO_2, CeO_2...) and turn out to be compatible with most of organic solvents and so assure a high level of catalyst dispersion in solution. The support is known to have a strong influence on the reactivity of AuNPs nanoparticles. So we expected that the very specific interaction between AuNPs and PTFE will led to new catalytic properties.

The preparation of PTFE immobilized AuNPs catalyst was preliminary evaluated by mixing commercially available PTFE microbeads (200 µm diameter) with the colloidal solution (Au concentration 3.3×10^{-4} mol.L^{-1}) resulting from the photochemical synthesis. Under such conditions; the hydrophobic PTFE powder remains on the water surface and did not disperse into the colloidal gold solution resulting in an inhomogeneous and extremely slow coloration of the support. The addition of acetone to the colloidal AuNPs solution (acetone-water 50/50 vol/vol) drove the microbeads into the liquid phase, leading to a full decolorizing of the initially purple solution after 4 hours under mechanical shacking. The catalyst is finally collected as a purple-grey powder by filtration and UV-Vis analysis of the filtrate demonstrated the absence of any absorption in the range of 400-700 nm confirming a complete immobilization of gold on PTFE surface. Assuming a complete deposition of AuNPs on PTFE surface lead to an amount of gold atoms per gram of PTFE powder of 3.3×10^{-5} $mol_{Au}.g^{-1}{}_{PTFE}$. The resulting powder has then been characterized by scanning electron microscopy (SEM) and X-ray photoelectron spectroscopy (XPS). With classical SEM apparatus, only larger particles with an average diameter of 30 nm can be observed immobilized on the PTFE surface. We presently suppose that AuNPs agglomerates during their immobilization on PTFE surface resulting in larger particles. Interestingly, SEM pictures show that larger particles are essentially located in on-surface roughnesses of the PTFE microbeads (Fig. 4). This particular localization strongly suggest that a stabilization effect occurs when the support surface recover AuNPs surface due to larger Au/F interactions.

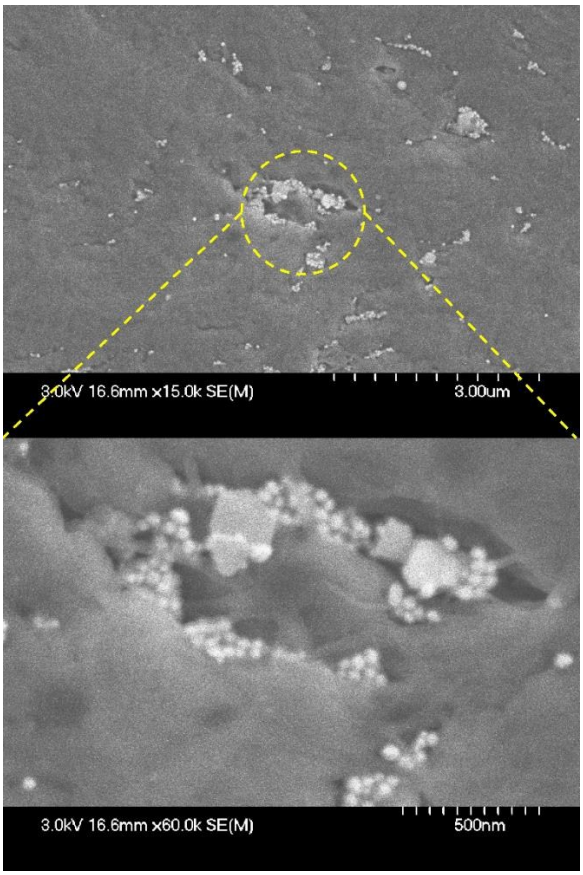

Fig. 4 SEM analysis of the PTFE immobilized AuNPs surface.

XPS analysis shows that compared to PTFE alone, PTFE immobilized AuNPs (AuNPs/PTFE) presents an absorption band specific from gold 4f orbital, confirming the absorption of AuNPs to the PTFE surface (Table 1, AuNPs/PTFE - Step 0). Au $4f^{7/2}$ binding energy (BE) of the AuNPs/PTFE is 84.8 eV, which falls in between $Au^{(0)}$ BE (83.8 eV)[33] and $Au^{(+I)}$ BE (85.0 eV),[34] suggests the coexistence of $Au^{(+I)}$ and $Au^{(0)}$ in the AuNP core (Fig. 5). Those results are in agreement with the continuous wave EPR analysis of AuNPs/PTFE performed at 5 K (Fig. 6). Indeed, EPR spectrum presents two main peaks corresponding to $Au^{(+I)}$ at 353 gauss and a second intense superparamagnetic peak at 113 gauss to $Au^{(0)}$ clusters respectively.

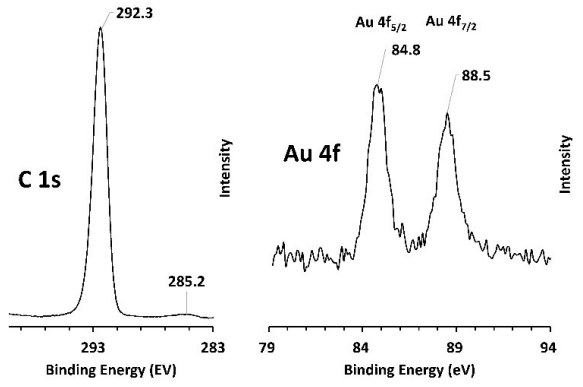

Fig. 5 AuNPs/PTFE XPS analysis (C(1s) and Au(4f) regions).

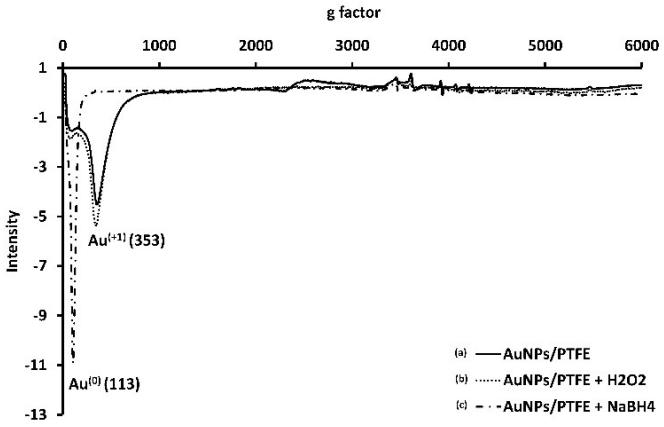

Fig. 6 AuNPs/PTFE EPR (5 K) spectra.

This hypothesis was confirmed by oxidation of AuNPs/PTFE in the presence of H_2O_2 resulting in a slight increase of the $Au^{(+I)}$ peak at 353 gauss on the EPR spectrum. Similarly under reductive conditions in the presence of $NaBH_4$ the EPR spectrum resulted in a complete disappearance of the $Au^{(+I)}$ peak and the formation of a unique superparamagnetic peak at 113 gauss corresponding to $Au^{(0)}$.

Analysis of the carbon region by XPS (Fig. 5 and Table 1, AuNPs/PTFE – Step 0), gave other fruitful information. PTFE is characterized by a single peak at 292.5 (+/- 0.1) eV attributed to CF_2 oligomers. When AuNPs are adsorbed on surface, a new peak at 285.2 (+/- 0.1) eV appears. As previous authors mentioned in literature this new peak could correspond to CF2 decomposition along AuNPs adsorption with formation of C-C bonds.[35, 36] Such peak is described to increase with the amount of adsorbed AuNPs suggesting a transformation of PTFE with AuNPs when anchoring. Here we suppose a fluorine abstraction with formation of radicals that rearrange on surface to form C-C bonds as recent literature mention the possibility to generate radicals from organic halides by halogen abstraction.[37, 38]

Table 1. X-ray photoelectron spectroscopy (XPS) quantitative analysis of the AuNPs/PTFE surface at different stages

Element	Orbital	AuNPs/PTFE (Step 0)[a]		AuNPs/PTFE (Step 1)[b]		AuNPs/PTFE (Step 2)[c]	
		BE (eV)	$\%_{atom}$	BE (eV)	$\%_{atom}$	BE (eV)	$\%_{atom}$
F	1s	689.7	68.40	689.5	67.15	689.3	66.48
O	1s	532.5	0.058	532.9	0.25	532.8	0.28
C	1s	292.5	31.56	292.4	32.39	292.4	33.04
	1s	285.2		285.2		285.2	
Au	$4f_{7/2}$	84.8	0.035	85.2	0.020	85.1	0.018
	$4f_{5/2}$	88.5		88.9		88.8	

[a] Step 0: AuNPs/PTFE after immobilization on surface.
[b] Step 1: AuNPs/PTFE after oxidative esterification.
[c] Step 2: AuNPs/PTFE after recycling conditions (H_2O_2/ Acetone / Water).

Oxidative esterification of aldehydes

Our catalyst in hand we evaluated it for the oxidative esterification of aromatic aldehydes in methanol. Preliminary aerobic experiments on benzaldehyde in the presence of AuNPS/PTFE (0.5% mol.) and a base demonstrated that at room temperature, molecular oxygen was not an appropriate co-oxidant for this reaction. This result is not surprising; as such oxidation conditions usually require high pressure of molecular oxygen to go to completion.[39]

We then decided to study the reaction in the presence of aqueous H_2O_2. A blank test, was first carried out in which the benzaldehyde oxidative esterification was performed in the presence of H_2O_2 (1.5 eq.) and NaOH (2 eq.) in methanol. The reaction showed an extremely slow reaction (Table 2, entry 1) with only 1% of methyl ester produced after 48 h. The GC/MS analysis shows that no Cannizaro reaction occurred in those conditions as no benzyl alcohol was detected. In presence of AuNPs/PTFE catalyst (Table 2, entry 2) the reaction gave a fair yield after 24 h. Optimization of the base (Table 2, entries 2-4) demonstrated that strong bases such as *t*-BuOK ($pK_{BH(H2O)}$ = 17.0) or NaOH powder/pellets ($pK_{BH(H2O)}$ = 15.7) were preferred to weaker organic bases such as DBU ($pK_{BH(H2O)}$ = 12.0), for which one no ester formation was observed even after 24 h. Strong bases which are able to quantitatively deprotonates methanol should accelerate the hemiacetal formation and the hydroperoxide anion formation required by the catalytic step. Because of its higher activity *t*-BuOK was chosen for the next experiments. The reaction appears very sensitive to temperature conditions (Table 2, entries 5-6). Interestingly yields are increased at lower temperatures. At the opposite at higher temperatures, the overall conversion dramatically drops traducing an inactivation of the catalytic system.

We observed in every catalytic experiment that gas bubbles appeared on AuNPs/PTFE surface. This could be explained by the formation of O_2 along H_2O_2 decomposition catalyzed by AuNPs as previously described by Scaiano and Garcia according to following equations:[40-43]

$$H_2O_2 + Au(0) \rightarrow HO^{\bullet} + HO^- + Au^+ \quad \text{Eq. 1}$$

$$HO^{\bullet} + H_2O_2 \rightarrow H_2O + HOO^{\bullet} \quad \text{Eq. 2}$$

$$HOO^{\bullet} + Au^+ \rightarrow O_2 + H^+ + Au(0) \quad \text{Eq. 3}$$

This side reaction which consumes H_2O_2, is accelerated by temperature which explains the observed yield decrease. For compensating H_2O_2 dismutation we multiplied its amount by two. The yield of methyl ester was higher but the yield of benzoic acid was also increased due to the introduction of larger amounts of water into the reaction medium (Table 2, entry 9). In order to achieve nearly complete conversions, we first increased the amount of catalyst (Table 2, entry 11). By doubling its amount the yield was increased by 20%. Finally we irradiated the mixture at room temperature with green fluorescent bulb centered on the plasmon resonance absorption band (LEXMAN EQSS-3 15 W, $\lambda = 525 \pm 30$ nm) which affords a further 5% increase (Table 2, entry 12).

In a next step the reaction was monitored by GC-MS. We observed a break in the kinetic rate after 19 minutes. Both parts of the kinetics follow an apparent zero order rate law with a reduced rate after 19 minutes. Under green irradiation the rate of oxidation reactions is accelerated and the break time is reduced to 15 minutes. The reaction is accelerated in the very first minutes and still follow an apparent zero order rate law. In the second part, the curve progress at the same rate for standard and irradiated conditions (Fig. 7). This reactivity can be explained by the formation of a reactive specie on AuNPs surface by H_2O_2 along very first minutes.

The second part of the curve can be explained by the presence of reactive oxygenated species resulting from H_2O_2 decomposition resulting in a second slower mechanism. The involvement of oxygen may be ruled out since the rate is not affected when the reaction is performed under a controlled atmosphere of argon. Successive addition of 1.5 equivalent of H_2O_2 every 20 minutes for standard conditions and every 15 minutes for photoactivated reaction maintained the reaction rate observed at the beginning of the reaction. This observation confirmed that H_2O_2 is the key element for generating the oxidative species on AuNPs surface. Under such repeated H_2O_2 additions conditions, the reaction went faster to completion and kept a constant zero order reaction rate (Table 3). The time to completion was reduced to 100 minutes under standard conditions and to only 45 minutes under green irradiation compared to 24 hours without repeated H_2O_2 additions.

Table 2. Benzaldehyde oxidative esterification catalyzed by AuNPs/PTFE

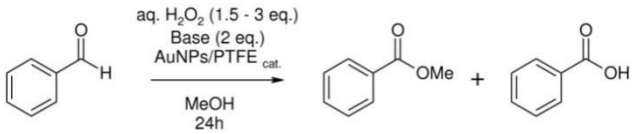

Entry[a]	Base	%cat.	Temp. (°C)	Light	Ester conv. (%)[b]	Acid conv. (%)[b]
1[c]	NaOH	-	25	No	1	-
2	NaOH	0.5	25	No	52	1
3	DBU	0.5	25	No	0	0
4	*t*-BuOK	0.5	25	No	56	1
5	*t*-BuOK	0.5	0	No	78	5
6	*t*-BuOK	0.5	65	No	3	0
9[d]	*t*-BuOK	0.5	25	No	67	6
10	*t*-BuOK	1	25	No	87	6
11	*t*-BuOK	1	25	Yes	92	7

[a] In a typical procedure, benzaldehyde (0.64 mmol), H_2O_2 (50% in H_2O, 1.5 eq.) and the base (2 eq.) were dissolved in MeOH (10 mL) for 30 minutes then the AuNPs/PTFE was added and the reaction was mixed under the desired light and temperature conditions for 24 h.

[b] Determined by GC-MS using internal standard.

[c] The reaction time was extended to 48 h.

[d] 3 eq. of H_2O_2 were used.

Table 3. Benzaldehyde oxidative esterification catalyzed by AuNPs/PTFE (1.0%) with repeated H_2O_2 additions

Entry[a]	$\%_{cat.}$	Light	Time (min)	Ester conv. (%)	Acid conv. (%)	k_{obs} ($mol.L^{-1}.s^{-1}$)
1	1	Room	100	92	8	1.16×10^{-5}
2	1	Sun[b]	30	72	-	2.55×10^{-5}
3	1	Green	30	>99	-	4.0×10^{-5}
4	0.25	Green	56	49	-	9.44×10^{-6}
5	0.5	Green	32	53	-	1.83×10^{-5}
6	0.75	Green	40	>99	-	3.25×10^{-5}

[a] In a typical procedure, benzaldehyde (0.64 mmol), H_2O_2 (50% in H_2O, 1.5 eq.) and *t*-BuOK (2 eq.) were dissolved in MeOH (10 mL) during 30 minutes then the AuNPs/PTFE was added and the reaction was mixed under the desired light conditions. Standard conditions: 1.5 eq. H_2O_2 added every 20 min.; Green light or sunlight conditions: 1.5 eq. H_2O_2 added every 8 min.

[b] Reaction temperature = 32 °C

Most of developed AuNPs based photocatalysts are usually combined with active composites or metal oxide supports[44] for which, based on experimental characterizations,[45] a concomitant electronic transfer from the AuNPs to the support after photon adsorption, similar to that of a dye-sensitized solar cell, is envisaged to explain a certain catalytic redox reactivity on the support itself.[46]

In our case, considering the inert character of PTFE support, such mechanism can't reasonably be envisaged and this remarkable light effect can be justified by generation of energetic and resonant electrons on AuNPs surface, after photon absorption, which strongly interact with the molecules adsorbed on the Au-NP surface and consequently enhance redox processes.

Interestingly, the selectivity toward the ester compared to acid under green irradiation and repeated additions of H_2O_2 is greatly enhanced as no trace of benzoic acid is observed. Such effect on the selectivity has recently been observed by Ke *et al.* along AuNPs photocatalyzed reductions.[47] These results highlights important opportunities of light driven catalysis for the improvement of chemical selectivity and reactivity by avoiding any by-product formation.

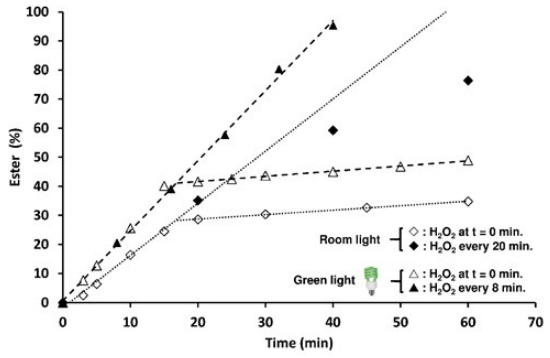

Fig. 7 Kinetic of benzoic acid methyl ester formation. Comparison between standard (◇), photocatalyzed (△), standard with repeated H_2O_2 additions (◆) and photocatalyzed with repeated H_2O_2 additions (□) conditions.

When the esterification reaction is fast, no formation of benzoic acid is observed until the reaction is complete. At longer times, under such basic conditions, a slow hydrolysis of methyl ester is usually observed.

Similarly when outer sunlight was used instead of the green light under optimum solar conditions and repeated additions of 1.5 equivalent of H_2O_2 every 8 minutes (Table 3, entry 2), the excellent selectivity for the ester was maintained. Despite higher temperature conditions (32 °C) a good reactivity was also conserved compared with the reaction done under fluorescent tubes room light (Table 3, entry 1), confirming the great potential of using sunlight instead of an artificial green light.

Then catalyst loading effect on the rate law has been studied in detail for benzaldehyde oxidative esterification (Table 3, entries 3-6, Fig. 8) and demonstrated as expected a linear relationship between the catalyst loading and the observed kinetic constant as expressed by the following equation:

$$k_{obs} = 4.09 \times 10^5 \times \%_{cat.} \qquad R^2 = 0.99$$

were k_{obs} is the observed kinetic constant expressed in $mol.L^{-1}.s^{-1}$ and $\%_{cat.}$ corresponds to the catalyst loading based on gold atoms in percentage.

Hammett relationships

To study the influence of electronic effects of the substrate on the reaction rate we established Hammett relationships on para-substituted benzaldehydes (Table 4). Reaction is slower for electron donating substituents and high conversions and full selectivity for the ester, is observed in every case. The observed rate constants are fitted by the classical σ substituent constants affording positive ρ Hammett value (ρ_{ox} = 2.35) with a good correlation factor (0.99) indicating that a partial negative charge is built up during the rate-determining step of the overall reaction pathway (Table 4 and Fig. 9, ● curve). Poor correlations were observed with Creary's substituent constants $\sigma_C^{\bullet}$ and modified substituent constants σ- or σ+. This result strongly suggest that the rate limiting step of the overall reaction pathway is the hemiacetal formation. Previously, Christensen *et al.* investigated such Hammett relationships in the aerobic oxidation of alcohols and aldehydes, catalyzed by Au/TiO_2.[48, 49] In the case of aldehyde oxidative esterification, for which no base was used compared to our system, the kinetics law was first order and only Creary's substituent constants for radical reaction ($\sigma_C^{\bullet}$) fitted with the kinetic data. However, if the *p*-CF_3 is removed, the data are fitted almost identically by the classical σ substituent constants.

The reported hemiacetal formation equilibria for substituted benzaldehydes in the presence of methanoate CH_3O^- has a large positive Hammett ρ value (ρ_{Hemi} = 3.20).[50, 51] In the absence of base, the reported hemiacetal formation equilibrium Hammett plot has a much lower ρ value (ρ_{Hemi} = 2.00) close to our measured value. Those two positive Hammett ρ values strongly suggest that the rate determining step of the reaction referred to the hemiacetalisation step.

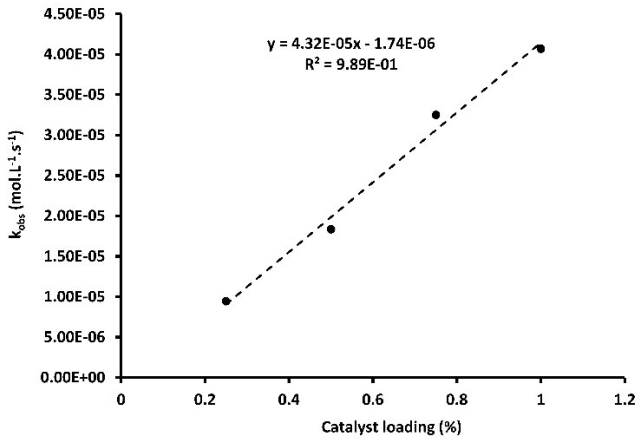

Fig. 8 Variation of k_{obs} of methyl benzoate formation at different catalyst concentrations (T = 25 °C, green irradiation).

In order to confirm this hypothesis we measured by ^{1}H NMR the hemiacetalisation equilibrium constants for the studied substituted benzaldehydes at the previous concentration (0.064 mol.L^{-1}) in CD_3OD and in the presence of 2 equivalents of *t*-BuOK as the base (Table 4). As shown in Figure 9, the corresponding Hammett plot presents a positive ρ value (ρ_{Hemi} = 2.31; R^2 = 0.98, ▲ curve) similar to the ρ_{ox} value observed for the photocatalyzed oxidative esterification, confirming that the hemiacetalisation step in this pathway is the rate determining step.

Table 4. Hammett study with AuNPs/PTFE (1%) and repeated H_2O_2 additions, under green light compared with benzaldehydes hemiacetalisation equilibria.

Substituent	σ	k_{obsX} (mol.L^{-1}.s^{-1}) [a]	$K_{hemi}x_{exp}$ [b]	Time (min)	Ester conv. (%)
p-OMe	-0.27	9.15×10^{-6}	5.00×10^{-2}	220	70
p-Me	-0.17	1.90×10^{-5}	1.10×10^{-1}	200	77
p-H	0.00	4.07×10^{-5}	2.90×10^{-1}	30	>99
p-F	0.05	6.25×10^{-5}	3.32×10^{-1}	30	>99
p-Cl	0.22	1.53×10^{-4}	6.70×10^{-1}	8	>99
p-Br	0.23	1.33×10^{-4}	8.69×10^{-1}	6	>99

[a] Measured by GC-MS after formic acid quenching. Kinetic constants have been defined as the average of two or three experiment measurement (see supplementary material). No trace of benzoic acids have been detected.
[b] Measured by ^{1}H NMR in CD_3OD.

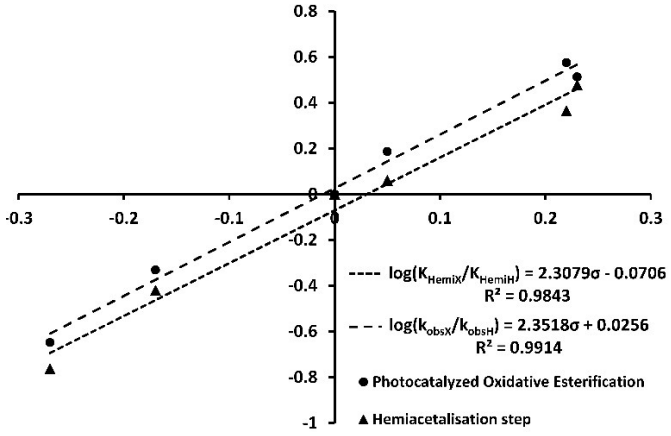

Fig. 9 Hammett plots for experimentally measured log (k_{obsX}/k_{obsH}) = 2.35 × σ + 0.026 (●) and log (K_{HemiX}/k_{HemiH}) = 2.31 × σ - 0.07 (▲).

Kinetic law

Kinetics results presented in Table 3 and Figure 7 exhibit an apparent zero order rate law. Hammett relationships strongly suggest the hemiacetalisation step as the rate limiting step, consequently the hemiacetalisation equilibrium constant (K_{Hemi}) should influence the kinetic law of the reaction. Heterogeneous catalytic reactions take place on surfaces as described by Eley-Rideal or Langmuir-Hinshelwood kinetic models.[52] Such mechanisms have already been envisaged in literature for other heterogeneous catalytic or photocatalytic reactions on AuNPs surface.[53] Eley-Rideal type mechanism describes heterogeneous catalyzed pathway which assume equilibrated adsorption of one reactant on catalyst surface followed by a subsequent reaction with a second reagent in solution.[54] In case of a Langmuir-Hinshelwood type mechanism, this time, equilibrated adsorption of two reactants on catalyst surface followed by their reactivity on surface has to be considered.[55]

Such mechanisms are usually admitted for gas phase reactions and rarely extended to liquid phase reaction.[56] In the present work an Eley-Rideal kinetic model is proposed in which hydrogen peroxyde acts as an oxidant in solution and where the hemiacetal anion is adsorbed on surface:

$$r_0 = -\frac{dC_{Benz}}{dt} = k_r C_S C_{H2O2} \frac{K_{Ads} K_{Hemi} C_{Benz}}{(1 + K_{Ads} K_{Hemi} C_{Benz})} \qquad \text{Eq. 4}$$

With:
k_r: kinetic constant for hemiacetal anion oxydation on surface
K_{Ads}: hemiacetal anion adsorption equilibrium constant
K_{Hemi}: hemiacetal anion formation equilibrium constant
C_S: surface gold atom concentration
C_{H2O2}: hydrogen peroxide concentration
C_{Benz}: benzaldehyde concentration

Because H_2O_2 is added continuously to the reaction medium, we considered its concentration constant along time, the kinetic model was consequently simplified and resulted in the following integrated form:

$$K_e C_{Benz} + \ln(C_{Benz}) = k_r C_S C_{H2O2} K_e t + K_e C_{0Benz} - \ln(C_{0Benz})$$

Giving:

$$C_{Benz} = K_e \omega \left\{ \frac{C_{0Benz}}{K_e} e^{\left(\frac{C_{0Benz} - k_r C_S C_{H2O2} K_e t}{K_e} \right)} \right\} \qquad \text{Eq. 6}$$

With: $K_e = K_{Ads} K_{Hemi}$ and ω: Lambert function

This model justify apparent zero order reaction rates for low hemiacetal anion adsorption equilibrium constants ($K_{Ads} < 10^{-4}$) and high k_r values ($k_r > 10^3$ s^{-1}). The hemiacetal equilibrium step affecting the overall K_e expression this model correlate with our preliminary assumption based on hemiacetalisation step as the rate determining step.

Proposed reaction mechanism

Christensen et al. suggest the formation of a radical anion deriving from the aldehyde to explain such correlation with an $H^{\bullet}$ abstraction occurring with e.g. an Au–O–O- specie in a radical recombination.

Assuming an Eley-Rideal type mechanism we may propose possible steps for the catalytic cycle (Fig. 10). Starting from AuNPs composed of $Au^{(0)}$ and $Au^{(+I)}$ atoms, under such basic conditions, hydrogen peroxide anion may oxidize AuNPs surface generating $Au^{(+I)}$-OH species and as previously envisaged by Barton along DFT studies $Au^{(+I)}$-O-O-$Au^{(+I)}$ intermediates.[57] This could be justified by the increase of oxygen quantity observed by XPS after the reaction (Table 1, AuNPs/PTFE - Step 1) or the increase of the $Au^{(+I)}$ peak at 353 gauss observed by EPR in the presence of H_2O_2. Then, an $Au^{(+I)}$-OH activated gold sites may be exchanged with a preformed hemiacetal anion, resulting from hemiacetalisation step between benzaldehyde and in-situ generated CH_3O^-. This substitution generating $Au^{(+I)}$-OCH(OCH_3)Ar catalytic intermediate and an equivalent of hydroxide anion acting later as a strong base along H_2O_2 deprotonation or even along hemiacetalisation step. The $Au^{(+I)}$-O-O-$Au^{(+I)}$ active center may then undergo an intramolecular hydride abstraction from adsorbed hemiacetal anion to generate by a concomitant electronic transfer on AuNPs surface hydroperoxide anion $Au^{(+I)}$-OOH intermediate, Au(0) and the corresponding desired ester. The formation of the minor benzoic acid side product can also be explained using this pathway by formation of an acetal in the presence of produced OH- instead of CH_3O- and its adsorption/oxidation on AuNPs surface. To close the catalytic cycle an equivalent of hydroperoxyde anion may regenerate $Au^{(+I)}$-O-O-$Au^{(+I)}$ and $Au^{(+I)}$-OH species on AuNPs surface to restart a new catalytic cycle. Existence of both hydroxide and hydroperoxide anions ($Au^{(+I)}$-OH and $Au^{(+I)}$-OOH) have been observed on AuNPs surface by XPS analysis by Falaras[58] and studied in detail by DFT calculation along the reaction mechanism of water formation from H_2 and O_2.[57] The formation of unusual $Au^{(+I)}$-O-O-$Au^{(+I)}$ catalytic center is justified in our case by the highly basic reactive medium.

The only difference in the green light enhanced reaction is the polarization of AuNPs which enhances the electronic transfer in the proposed mechanism. In accord with the Hammett ρ value the rate limiting step in this overall pathway corresponds to the hemiacetalisation formation. The oxidation step on AuNPs surface should be considered as fast as proposed by the Eley-Rideal kinetic model.

Recycling of the catalyst

The AuNPs/PTFE catalyst is perfectly stable after preparation and may be stored for weeks. We tested the recycling of AuNPs/PTFE catalyst in the oxidative esterification of benzaldehyde. After the first benzaldehyde oxidative esterification, the catalyst was separated from the reaction mixture by filtration, thoroughly washed with methanol, and then reused as catalyst for the next run under the same conditions. Along the second run, the conversion drops to 59% after a longer reaction time of 45 minutes and the catalyst appears inactive along the third run. Observation of the catalyst after each step under a stereomicroscope demonstrated a change in the polymer shape (plates instead of beads). When the catalyst (250 mg) is treated for 2 hours with a solution of H_2O_2 (300 µL, 50%w in water) and acetone (5 mL) in water (5 mL), filtrated, and washed with methanol, as shown in Figure 11, the methyl ester yields remained quantitative and constant for the ten successive cycles. This result reflects the high stability and reusability of the regenerated catalyst. Surprisingly, when the catalyst is reactivated using this procedure, kinetic measurements demonstrated that for every successive run the selectivity is complete for the ester and that a zero order rate law is still observed. Furthermore the reaction is accelerated and complete after only 24 minutes compared to 30 minutes under standard conditions.

Interestingly for every runs, a delay of 8 minutes is also observed before the beginning of the reaction suggesting a pre-activation of AuNPs surface under such new conditions. This delay shows also an exceptional reactivity (only 16 minutes of oxidation time) after pre-activation. When the AuNPs/PTFE is treated with H_2O_2/acetone after each reaction step no change in the shape of the polymer beads is observed even after 10 cycles. This surface activation could be justified by *in-situ* formation of a very reactive diluted triacetonetriperoxide species[59] along reactivation treatment generating unidentified highly reactive intermediates on AuNPs surface. Nevertheless, XPS analysis of the treated AuNPs catalyst (Table 1, AuNPs/PTFE - Step 2) didn't show any significant change compared to the AuNPs catalyst after reaction without recycling treatment (Table 1, AuNPs/PTFE - Step 1).

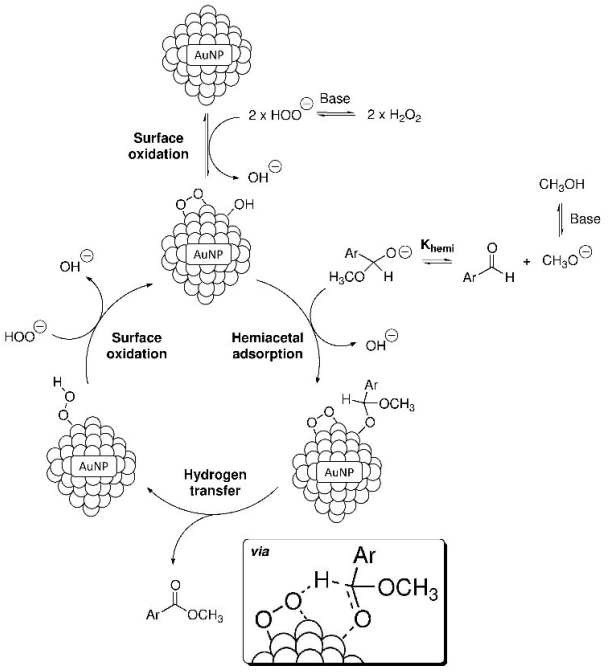

Fig. 10. Schematic mechanisms of the reaction pathways in the photocatalytic oxidative esterification of aromatic aldehydes by AuNPs/PTFE in the presence of H_2O_2 and a strong base.

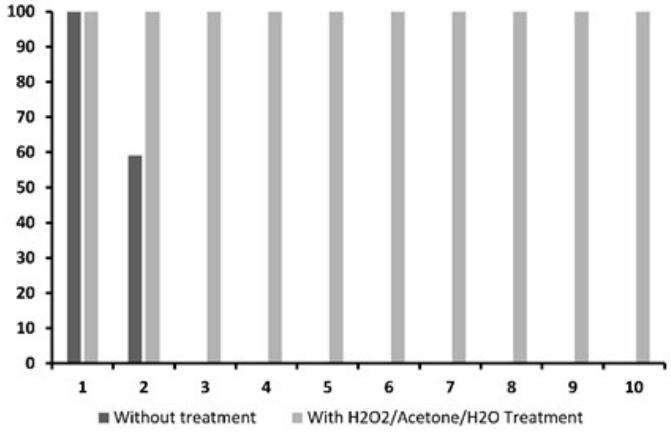

Fig. 11 Recycling of the AuNPs/PTFE catalyst ($1\%_{cat}$) for the photocatalyzed oxidative esterification of benzaldehyde under repeated additions of H_2O_2 every 8 minutes. (■) without reactivation treatment between two runs; (■) with H_2O_2 (50%) / Acetone / water treatment between 2 runs. The conversion is measured at 45 minutes by GC-MS.

By comparison with previously reported oxidative esterification reactions catalyzed by gold nanoparticles immobilized on various mineral supports in the presence of O_2[60-64] our catalytic system appears more stable and more active after the recycling step. Indeed, by comparison with most of mineral supports usually evaluated, the catalyst preparation is usually complex and its activity usually decreases after few cycles. To our knowledge, from the best recyclable AuNPs catalysts, Au-K_2CO_3 reported by Gao[65] was reused 8 times without loss of activity but by comparison our mild catalytic system requires less energy (15 W light instead of usual high temperatures or high O_2 pressures) and appears much faster than most of catalytic systems using O_2 as the co-oxidant.

Conclusions

Homogeneous unstabilized gold nanoparticles (AuNPs) of 1 to 2 nm diameter were obtained by photochemical reduction of $Au^{(3+)}$ solution by a high intensity UV LED source. These AuNPs supported on polytetrafluoroethylene (PTFE) are an efficient catalyst for the photocatalytic oxidative esterification of aldehydes with aqueous hydrogen peroxide under mild conditions. The inert nature of PTFE polymer allowed us to work in hydrophobic solvents in nearly anhydrous conditions, which led to a nearly absence of formation of benzoic acid.

Hammett free energy relationship study demonstrated that hemiacetalisation equilibrium is the rate limiting step. The overall reaction obeys a zero order rate law which follows an Eley-Rideal model, based on previously described intermediates, a catalytic cycle on gold surface is proposed.

The recycling study opened the way to new and efficient regenerating conditions for AuNPs catalysts and the exceptional reactivity of such new catalyst has to be elucidated. Furthermore, preliminary results seems to show an important effect of the AuNPs size, measured after their photochemical synthesis, on catalytic activity, these results will be reported in due course. Further work is necessary to rationalize this effect.

Parallel to this work, we recently described, the transposition of batch reaction into AuNPs immobilized capillary flow reactors allowing a better control of the reaction. The design of AuNPs/PTFE based catalytic microreactors is of high interest, and will be reported in due course. Further extension of the present H_2O_2–AuNPs/PTFE catalytic system to other key oxidative transformations is currently being explored. In summary AuNPs supported on PTFE extend the traditional support of AuNPs and have great potential as photocatalyst for the development of environmentally benign reactions.

Acknowledgements

This work was supported by the Conseil Régional Nord, Pas-de-Calais, France. The NMR and Mass Spectrometry facilities used in this study were funded by the European Community (FEDER), the Région Nord-Pas de Calais (France), the CNRS, and the Université de Lille. MP thanks the Region Nord-Pas de Calais for a Young Investigator Grant funded by the Contrat de Projet État-Région (CPER) to the Institut Michel E. Chevreul (FR CNRS 2638). The authors thank Mr. Fredrik Ljungkvist for performing recycling experiments, Dr. Alexandre Mussi for his help in performing the microscope study, Pr. Patrice Woisel for giving us a generous access to their DLS instrument and Dr. Maria van Agthoven for her help with editing this manuscript.

Notes and references

1 M. B. Smith and J. March, *March's advanced organic chemistry: reactions, mechanisms, and structure*, John Wiley & Sons, 2007.

2 R. C. Larock, *Comprehensive organic transformations: a guide to functional group preparations*, Wiley-VCH New York, 1999.

3 K. Ekoue-Kovi and C. Wolf, *Chemistry-A European Journal*, 2008, **14**, 6302-6315.

4 M. Haruta, T. Kobayashi, H. Sano and N. Yamada, *Chemistry Letters*, 1987, 405-408.

5 Y. Zhang, X. Cui, F. Shi and Y. Deng, *Chemical reviews*, 2011, **112**, 2467-2505.

6 Z. Li, C. Brouwer and C. He, *Chemical reviews*, 2008, **108**, 3239-3265.

7 A. Corma and H. Garcia, *Chemical Society Reviews*, 2008, **37**, 2096-2126.

8 C. Della Pina, E. Falletta, L. Prati and M. Rossi, *Chemical Society Reviews*, 2008, **37**, 2077-2095.

9 E. Taarning, I. S. Nielsen, K. Egeblad, R. Madsen and C. H. Christensen, *ChemSusChem*, 2008, **1**, 75-78.

10 I. S. Nielsen, E. Taarning, K. Egeblad, R. Madsen and C. H. Christensen, *Catalysis Letters*, 2007, **116**, 35-40.

11 H. Miyamura, T. Yasukawa and S. Kobayashi, *Green Chemistry*, 2010, **12**, 776-778.

12 T. Hayashi, T. Inagaki, N. Itayama and H. Baba, *Catalysis today*, 2006, **117**, 210-213.

13 A. Corma and M. E. Domine, *Chemical communications*, 2005, 4042-4044.

14 J. Ni, W.-J. Yu, L. He, H. Sun, Y. Cao, H.-Y. He and K.-N. Fan, *Green Chemistry*, 2009, **11**, 756-759.
15 D. Philip, *Spectrochimica Acta Part A: Molecular and Biomolecular Spectroscopy*, 2008, **71**, 80-85.
16 D. Tsukamoto, Y. Shiraishi, Y. Sugano, S. Ichikawa, S. Tanaka and T. Hirai, *Journal of the American Chemical Society*, 2012, **134**, 6309-6315.
17 S.-i. Naya, A. Inoue and H. Tada, *Journal of the American Chemical Society*, 2010, **132**, 6292-6293.
18 A. Primo, A. Corma and H. García, *Physical Chemistry Chemical Physics*, 2011, **13**, 886-910.
19 H. Zhu, X. Chen, Z. Zheng, X. Ke, E. Jaatinen, J. Zhao, C. Guo, T. Xie and D. Wang, *Chem. Commun.*, 2009, 7524-7526.
20 J. Ftouni, M. Penhoat, A. Addad, E. Payen, C. Rolando and J.-S. Girardon, *Nanoscale*, 2012, **4**, 4450-4454.
21 J. Ftouni, M. Penhoat, J.-S. Girardon, A. Addad, E. Payen and C. Rolando, *Chemical Engineering Journal*, 2013, **227**, 103-110.
22 F. Pinna, *Catalysis Today*, 1998, **41**, 129-137.
23 M. M. Maye, J. Luo, L. Han, N. N. Kariuki and C.-J. Zhong, *Gold Bulletin*, 2003, **36**, 75-82.
24 J. C. Scaiano, K. G. Stamplecoskie and G. L. Hallett-Tapley, *Chemical Communications*, 2012, **48**, 4798-4808.
25 K. L. McGilvray, M. R. Decan, D. Wang and J. C. Scaiano, *Journal of the American Chemical Society*, 2006, **128**, 15980-15981.
26 M. L. Marin, K. L. McGilvray and J. C. Scaiano, *Journal of the American Chemical Society*, 2008, **130**, 16572-16584.
27 M. Brust, M. Walker, D. Bethell, D. J. Schiffrin and R. Whyman, *Journal of the Chemical Society, Chemical Communications*, 1994, 801-802.
28 W. W. Weare, S. M. Reed, M. G. Warner and J. E. Hutchison, *Journal of the American Chemical Society*, 2000, **122**, 12890-12891.
29 Z. Wang, Q. Zhang, D. Kuehner, A. Ivaska and L. Niu, *Green Chemistry*, 2008, **10**, 907-909.
30 K. L. Mittal, *Metallized Plastics*, Springer, 1991.
31 L. M. Siperko and R. R. Thomas, *Journal of adhesion science and technology*, 1989, **3**, 157-173.
32 E. Redel, M. Walter, R. Thomann, C. Vollmer, L. Hussein, H. Scherer, M. Krüger and C. Janiak, *Chemistry-A European Journal*, 2009, **15**, 10047-10059.
33 K. Dückers and H. P. Bonzel, *Surface Science*, 1989, **213**, 25-48.
34 M. P. Casaletto, A. Longo, A. Martorana, A. Prestianni and A. M. Venezia, *Surface and Interface Analysis*, 2006, **38**, 215-218.
35 J. Perrin, B. Despax and E. Kay, *Physical Review B*, 1985, **32**, 719-732.
36 N. Cioffi, I. Losito, L. Torsi, I. Farella, A. Valentini, L. Sabbatini, P. Zambonin and T. Bleve-Zacheo, *Chemistry of Materials*, 2002, **14**, 804-811.
37 J. Sá, A. Goguet, S. Taylor, R. Tiruvalam, C. J. Kiely, M. Nachtegaal, G. J. Hutchings and C. Hardacre, *Angewandte Chemie*, 2011, **123**, 9074-9078.
38 P. Ionita, M. Conte, B. C. Gilbert and V. Chechik, *Organic & biomolecular chemistry*, 2007, **5**, 3504-3509.
39 R. L. Oliveira, P. K. Kiyohara and L. M. Rossi, *Green Chemistry*, 2009, **11**, 1366-1370.
40 S. Navalon, R. Martin, M. Alvaro and H. Garcia, *Angewandte Chemie*, 2010, **122**, 8581-8585.
41 S. Navalon, M. de Miguel, R. Martin, M. Alvaro and H. Garcia, *Journal of the American Chemical Society*, 2011, **133**, 2218-2226.
42 P. Montes-Navajas and H. García, *The Journal of Physical Chemistry C*, 2010, **114**, 18847-18852.
43 G. L. Hallett-Tapley, M. J. Silvero, M. González-Béjar, M. Grenier, J. C. Netto-Ferreira and J. C. Scaiano, *The Journal of Physical Chemistry C*, 2011, **115**, 10784-10790.
44 X. Zhou, G. Liu, J. Yu and W. Fan, *Journal of Materials Chemistry*, 2012, **22**, 21337-21354.
45 Y. Tian and T. Tatsuma, *Journal of the American Chemical Society*, 2005, **127**, 7632-7637.
46 W. Hou and S. B. Cronin, *Advanced Functional Materials*, 2013, **23**, 1612-1619.
47 X. Ke, X. Zhang, J. Zhao, S. Sarina, J. Barry and H. Zhu, *Green Chemistry*, 2013, **15**, 236-244.
48 P. Fristrup, L. B. Johansen and C. H. Christensen, *Chemical Communications*, 2008, 2750-2752.
49 P. Fristrup, L. B. Johansen and C. H. Christensen, *Catalysis Letters*, 2008, **120**, 184-190.
50 P. Zuman, *Arkivoc*, 2002, **1**, 85-140.
51 M. Arora, B. G. Cox and P. E. Sorensen, *Journal of the Chemical Society, Perkin Transactions 2*, 1979, 103-107.
52 R. Baxter and P. Hu, *The Journal of chemical physics*, 2002, **116**, 4379-4381.
53 S. Brosillon, L. Lhomme, C. Vallet, A. Bouzaza and D. Wolbert, *Applied Catalysis B: Environmental*, 2008, **78**, 232-241.
54 D. Eley and E. Rideal, Proceedings of the Royal Society of London A: Mathematical, Physical and Engineering Sciences, 1941.
55 L. Glasser, *Journal of Chemical Education*, 1979, **56**, 22.
56 S. Wunder, Y. Lu, M. Albrecht and M. Ballauff, *Acs Catalysis*, 2011, **1**, 908-916.
57 D. G. Barton and S. G. Podkolzin, *The Journal of Physical Chemistry B*, 2005, **109**, 2262-2274.
58 I. Arabatzis, T. Stergiopoulos, D. Andreeva, S. Kitova, S. Neophytides and P. Falaras, *Journal of Catalysis*, 2003, **220**, 127-135.
59 M. E. Sigman, C. D. Clark, T. Caiano and R. Mullen, *Rapid Communications in Mass Spectrometry*, 2008, **22**, 84-90.
60 F. Z. Su, J. Ni, H. Sun, Y. Cao, H. Y. He and K. N. Fan, *Chem. Eur. J.*, 2008, **14**, 7131-7135.
61 K. Suzuki, T. Yamaguchi, K. Matsushita, C. Iitsuka, J. Miura, T. Akaogi and H. Ishida, *ACS Catal.*, 2013, **3**, 1845-1849.

62 X. Wan, W. Deng, Q. Zhang and Y. Wang, *Catal. Today*, 2014, **233**, 147-154.
63 P. Mondal, N. Salam, A. Mondal, K. Ghosh, K. Tuhina and S. M. Islam, *J. Colloid Interface Sci.*, 2015, **459**, 97-106.
64 H. Wei, J. Li, J. Yu, J. Zheng, H. Su and X. Wang, *Inorg. Chim. Acta*, 2015, **427**, 33-40.
65 L. Wang, J. Li, W. Dai, Y. Lv, Y. Zhang and S. Gao, *Green Chem.*, 2014, **16**, 2164-2173.

Graphical Abstract:

Fast and mild visible light photocatalytic conditions for oxidative esterification of aldehydes using H_2O_2 and AuNPs/PTFE catalyst.